

Relevance of the Computational Models of Bacterial Interactions in the simulation of Biofilm Growth

Gabriel Santos-Díaz¹, Álvaro Rodríguez-Rivas³, and Alejandro Cuetos^{1,2*}

¹*Department of Physical, Chemical and Natural Systems, Pablo de Olavide University, Seville, Spain*

²*Center for Nanoscience and Sustainable Technologies (CNATS), Pablo de Olavide University, Seville, Spain and*

³*Departamento de Física Aplicada I, Escuela Politécnica Superior, Universidad de Sevilla, 41011, Seville, Spain*

This study explores the application of elongated particle interaction models, traditionally used in liquid crystal phase research, in the context of early bacterial biofilm development. Through computer simulations, using an agent based model, of the repulsive and attractive of Kihara models and Hertz interaction model, we investigate the possibilities and limitations for modelling biofilm formation and growth. Our approach focuses on understanding how mechanical forces due to the interaction between cells, in addition to growth and diffusive parameters, influence the formation of complex bacterial communities. By comparing such force models, we evaluate their impact on the structural properties of bacterial microcolonies. The results indicate that, although the specific force model has some effect on biofilm properties, the intensity of the interaction between bacteria is the most important determinant. This study highlights the importance of properly selecting interaction strength in simulations to obtain realistic representations of biofilm growth, and suggests which adapted models of rod-shaped bacterial systems may offer a valid approach to study the dynamics of complex biofilms.

Keywords: Individual-based model, Brownian dynamics simulation, Bacterial self-assembly, Biofilm growth, Kihara potentials, Hertz model

I. INTRODUCTION

In theoretical and simulation studies, the way of modelling the interaction between the agents (molecules, colloidal particles, etc.) that constitute the system has always been recognised as a fundamental element. In the late 20th and early 21st centuries, the choice between the different models available was a major issue in the scientific literature. At that time, it was crucial to clarify whether the different options to choose from were able to realistically reproduce the complexity of experimental observations. This was especially relevant in the field of simulation and theoretical studies of non-spherical particle fluids, such as linear hydrocarbons, or prolate and oblate mesogens, where several models have been proposed as tools for the systematic study of complex fluids by means of computer simulation [1–8]. Following these ideas, we present in this work a systematic study of the choice of some of these models for the modelling and simulation of cell colonies. Specifically, in this work we focus on the study by means of computer simulation of the development of bacterial biofilms.

Bacterial biofilms are the most common form of bacterial communities. They consist of bacterial assemblages that, often starting from a single cell and through the process known as binary fission, can form complex structures of millions of individuals. To understand the formation and development of these communities several aspects must be taken into consideration. These include environmental factors such as nutrient and harmful chem-

ical concentrations, the substrate on which the colony grows, or the presence of other bacterial species, among others [9, 10]. In reaction to these conditions, cells exhibit various physiological responses that are typically genetically controlled and mediate their reactions to different environmental interactions.

Traditionally, the study of bacteria and biofilm responses to external stimuli has focused on the characteristics of the chemical environment in which cells grow. However, in recent years, there has been growing interest in the mechanical aspects of bacterial and biofilm responses [11–13]. For instance, the movement of bacteria in bulk fluids, where hydrodynamic interactions with other cells and flow play a vital role [12, 14], or the rheological properties of biofilms [12, 13, 15–17]

The mechanical response of individual bacteria and biofilms to applied forces and stresses is also an important factor to consider. For instance, there is ample evidence that growth-induced pressure results in a reduction in the rate of cell growth and reproduction in cellular ensembles. This effect has been observed in populations of microorganisms, such as yeast [18, 19] and bacteria [20–22], as well as in tissues [23, 24] and tumors [25, 26]. The ability of bacteria to respond to mechanical stimuli could be attributed to two key factors. Firstly, the presence of mechanotransduction systems in the bacterial wall facilitates the conversion of mechanical inputs into cellular responses [27, 28]. Secondly, the interactions between cells and their environment, as well as between different cells. In this sense various types of forces have been identified at different stages of biofilm development [29, 30]. Surface forces, comprising electrostatic and van der Waals interactions, lubrication forces, or the so-called fimbrial forces [31, 32]. All these interactions can be repulsive or

*Electronic address: acuemen@upo.es

attractive.

In recent times, considerable effort has been focused on creating models and simulations to better understand the growth and development of biofilms, as well as other cellular communities such as tissues and tumors. Among the various approaches proposed, a subject on which it is possible to find very interesting reviews in the literature [33–35], Individual-Based Models (IbM) have gained considerable attraction and attention as an effective tool for studying these complex systems [33, 36–40]. This approach suggests that the process of growth in a cell community, from microcolonies to biofilms in the case of bacteria, can be effectively characterized by analysing the key attributes of individual bacteria and the interactions between them. In IbM models it is possible to track and quantify the properties of each individual cell, which is one of their main advantages. In these models, the key ingredients are cell elongation and division, in some cases modulated by nutrient consumption, and an overdamped Brownian dynamics to simulate bacterial movement. It is in these dynamic equations where forces between cells and with other elements such as walls or obstacles must be introduced [41, 42]. In this context different mathematical models have been employed, aiming to capture the phenomenology of the forces between cells described above [37]. These models include linear springs [43], or repulsive forces proportional to contact area [44, 45], to cite some early examples.

Possibly the most employed model is the derived from the Hertz theory of elastic contact [46]. This model has often been used to estimate the force between two bacteria in contact [37, 47–49]. The main limitation of this model in this context is that it has been proposed for spherical particles in contact, and therefore does not take into account the elongated shape of bacteria. Another limitation of the Hertz model is that, even with total overlap between the two cells, the force maintains a finite value. Although this is partly compensated for by the high value of Young’s modulus found for bacteria [50], the smoothness of the interaction makes it necessary to use very small time steps in computer simulation studies to avoid unrealistic overlaps between cells. The possibility of such spurious overlaps is more relevant in the simulation of compact colonies, where, as noted above, the self-induced stress can be very high.

As an alternative to the Hertz model, our group has recently proposed the use of models commonly used in other contexts, such as the study of elongated particle fluids. Thus, we have proposed the use of spherocylindrical models such as the Soft Repulsive Spherocylindrical (SRS) model [7, 51–53] or the Kihara potential [6, 54] for modelling early biofilm development using IbM scenarios [39, 55–57]. These models have the advantage of naturally introducing the spherocylindrical shape observed in rod-shaped bacteria. Moreover, these models rapidly become more repulsive as the overlap between interacting particles increases, thus imposing a constraint on this possibility. On the other hand, the main limitation for

their use in the context of cellular simulation is that there is no physical reason to assume that these models reflect the functional form of steric interaction between two cells, beyond possible similarities with molecular or colloidal systems.

In any case, to the best of our knowledge, there are aspects of the use of possible cell-cell interaction models that previous studies have not clarified. For example, there is the basic question of whether the choice of one force model over another, beyond its physical realism, has a significant effect on the collective properties of cell colonies as observed by simulation. This would include testing the effect of the greater or lesser smoothness of the interaction, as well as the possible existence of attractive contact forces in addition to the repulsive forces due to steric interaction. To explore this issue, we have compared the properties of microcolonies generated by simulation when modelling bacteria interaction with the Hertz model, the SRS or repulsive Kihara interaction potential or, in contrast to the repulsive nature of these two models, the Kihara potential which additionally presents an attractive contribution. Our main objective is to elucidate the importance of choosing a particular cell-cell interaction model when proposing an agent-based algorithm for modelling biofilm development. We believe that this is an important aspect, and that it will be of considerable help to researchers interested in implementing models for the study of cellular communities. We also want to elucidate the effect of the strength of the interaction between bacteria, to determine the weight and relevance this parameter may have on the collective properties of the cell colonies. As in previous work [39, 55, 57], we focus on the case of early microcolonies when they are still two-dimensional. We understand that our conclusions are valid and extendable to later situations, where colonies are more complex and three-dimensional.

II. METHODS

The simulation methodology employed in this work has many points in common with our previous work on biofilm simulation [39, 55, 57]. It should be noted that, as discussed in these previous studies, our model does not explicitly introduce relevant aspects such as the EPS matrix or the effect of water, these factors being considered implicit in the model parameters. We highlight here the most relevant details. As in previous studies, we have focused on the early stages of biofilm development, when microcolonies can be considered two-dimensional systems. In these stages, bacterial biofilms have the particularity that in the early stages of their development they are two-dimensional structures, evolving to three-dimensional systems in later stages of their development [49]. In addition, experimental setups have been described in which biofilms develop confined between two surfaces, always being two-dimensional [21]. Accordingly, rod-like bacteria have been modelled as the

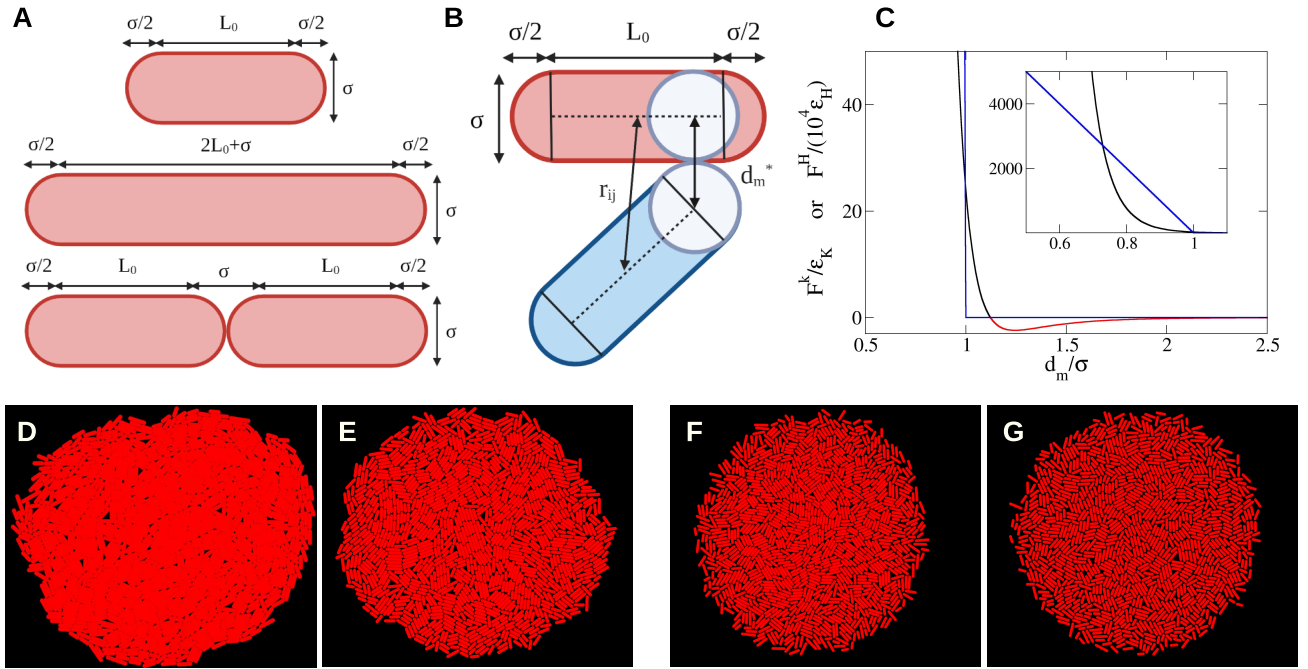


FIG. 1: (A) Schematic representation of the geometrical parameters of the bacterial model. (B) Parameters involved in the calculation of the forces in Kihara and Hertz models (see main text for details). (C) Comparison between the modulus of the forces calculated by repulsive and attractive Kihara models (F^K/ϵ_K , black and red line respectively), and Hertz model ($F^H/10^4 \epsilon_H$, blue line) as function of the minimum distance between cells d_m/σ . The inset shows a zoom to the region of $d_m/\sigma \in [0.5, 1.1]$. (D)-(G) Configurations of microcolonies with biomass $m(t) \approx 3500$ obtained with repulsive Kihara model with $\epsilon_K/k_B T = 1$ (D and F) and $\epsilon_K/k_B T = 100$ (E and G), at $\Gamma = 10$ (D and E) and $\Gamma = 0.1$ (F and G).

two-dimensional projection of the spherocylindrical particles. This kind of particle consists of a cylinder of instantaneous elongation L capped by two hemispheres of diameter σ , the latter will be considered as the unit of length along this study. During the simulation, the diameter of the particles is going to remain constant, while the elongation of the cylinder will change over time. Thus, the elongation of the cylindrical part of a given particle grows exponentially, following the expression $L(t) = L^i \cdot \exp(r^i \cdot (t - t_0))$. Here r^i is the elongation rate of the bacterium i . t_0 is the instant when the last division occurred for bacterium i . r^i is chosen at random from a Gaussian distribution centred at r and relative standard deviation $s/r = 0.1$. This exponential growth occurs from an initial elongation L_0 . A time-dependent aspect ratio can then be defined for each bacterium as $L_i^*(t) = L_i(t)/\sigma + 1$. We will denote the initial aspect ratio as L_0^* . In this growth process, when a bacterium reaches an aspect ratio of $L_f^* = 2L_0^* = 2(L_0/\sigma + 1)$ it splits into two identical particles, each with aspect ratio L_0^* [39, 57]. The lengthening and division process is repeated from here for the two resulting cells. This process, as well as the main geometrical parameters describing the cells, are sketched in Fig.1-A.

In addition to size, the position and orientation of the bacteria also evolves over time. This evolution has been

simulated, as in previous work [39, 55, 57], using Brownian dynamics, which incorporates both Brownian fluctuations in the position and orientation of the cells, as well as the motion caused by the interaction between the bacteria. Thus, the trajectory of the centre of mass and orientation of its longitudinal axis of an individual bacterium i , defined by the vectors \mathbf{r}_i and \mathbf{u}_i , evolves in the time according to the following set of equations:

$$\mathbf{r}_i^{\parallel}(t + \Delta t) = \mathbf{r}_i^{\parallel}(t) + \frac{D_{i\parallel}}{k_B T} \mathbf{F}_i^{\parallel}(t) \Delta t + (2D_{i\parallel} \Delta t)^{1/2} R^{\parallel} \hat{\mathbf{u}}_i(t) \quad (1)$$

$$\mathbf{r}_i^{\perp}(t + \Delta t) = \mathbf{r}_i^{\perp}(t) + \frac{D_{i\perp}}{k_B T} \mathbf{F}_i^{\perp}(t) \Delta t + (2D_{i\perp} \Delta t)^{1/2} R^{\perp} \hat{\mathbf{v}}_i(t) \quad (2)$$

$$\hat{\mathbf{u}}_i(t + \Delta t) = \hat{\mathbf{u}}_i(t) + \frac{D_{i\vartheta}}{k_B T} \mathbf{T}_i(t) \times \hat{\mathbf{u}}_i(t) \Delta t + (2D_{i\vartheta} \Delta t)^{1/2} R^{\vartheta} \hat{\mathbf{v}}_i(t) \quad (3)$$

being \mathbf{r}_i^{\parallel} and \mathbf{r}_i^{\perp} the projections of \mathbf{r}_i on the directions

parallel and perpendicular to $\hat{\mathbf{u}}_i$, respectively. \mathbf{F}_i^{\parallel} and \mathbf{F}_i^{\perp} are the parallel and perpendicular components of the total force acting on i and \mathbf{T}_i is the total torque due to the interactions with other particles of the fluid [58]. The brownian dynamic is induced through a set of independent gaussian random numbers of variance 1 and zero mean: R^{\parallel} , R^{\perp} and R^{ϑ} . $\hat{\mathbf{v}}_i$ is an unitary vector perpendicular to $\hat{\mathbf{u}}_i$. In this equations k_B is the Boltzmann constant, and T the temperature. Δt is the time step.

For the diffusion coefficients, $D_{i\parallel}$, $D_{i\perp}$ and $D_{i\vartheta}$, as in previous works [57] we have employed expressions calculated by a method similar to that proposed by Bonet Avalos and co-workers [59]. These diffusion coefficients depend on the size of the particles and they must be calculated for each bacterium at each time step. The explicit expressions for the calculation of these diffusion coefficients for a given aspect ratio are:

$$\begin{aligned} D_{\parallel}/D_0 &= -0.0198 \cdot \ln(L^*) + 0.0777 + \frac{0.0437}{L^*} \\ &\quad - \frac{0.0158}{L^{*2}} \\ D_{\perp}/D_0 &= -0.0119 \cdot \ln(L^*) + 0.0452 + \frac{0.0796}{L^*} \\ &\quad - \frac{0.0190}{L^{*2}} \\ D_{\vartheta}\sigma^2/D_0 &= -0.0002 \cdot \ln(L^*) + 0.0012 - \frac{0.0243}{L^*} \\ &\quad + \frac{0.3233}{L^{*2}} + \frac{0.2597}{L^{*3}} - \frac{0.0483}{L^{*4}} \end{aligned} \quad (4)$$

depending on the diffusional parameter $D_0 = D_0^*\sigma^2/\tau$, with τ the time unit.

An important aspect of our work is how to model the forces between bacteria. As mentioned in the introduction, one of the aims of this study is to compare the effects of using one or the other model to represent the forces. As discussed there, in this paper we have chosen to compare two of the models that have been employed in the past in modeling the interaction between cells. On the one hand, Kihara models, with and without attractive part. On the other hand, the Hertz elastic force model. We proceed to present both models in detail.

The Kihara interaction potential [6, 54] is a model used in the past to simulate the liquid crystal phase diagram of rod-like particles. The mathematical expression of this potential is:

$$U_{ij} = \begin{cases} 4\varepsilon_K \left[\left(\frac{1}{d_m^*}\right)^{12} - \left(\frac{1}{d_m^*}\right)^6 - E_{cu} \right] & d_m \leq d_{cu} \\ 0 & d_m > d_{cu} \end{cases} \quad (5)$$

where i and j are generic particles (bacteria). $d_m^* = d_m/\sigma$ is the shorter distance between them, calculated as the minimum distance between two spherocylinders (see Fig. 1-B) [60]. d_{cu} is the distance at what the interac-

tion is truncated and shifted, and $E_{cu} = d_{cu}^{*-12} - d_{cu}^{*-6}$. If $d_{cu} \leq \sqrt[6]{2}\sigma$ the interaction is purely repulsive, while if d_{cu} is bigger than this value the interaction is attractive for interparticle distances bigger than $\sqrt[6]{2}\sigma$. ε_K represents the strength of the interaction in the Kihara models. In this study d_{cu} has been set to $\sqrt[6]{2}\sigma$ for the repulsive Kihara models, and 2.5σ for the attractive Kihara models. From this expression of the interaction potential is easy to obtain the forces and torques required in equations 1 to 3 [58]. Specifically, the explicit expression for the force that particle i exerts on particle j is

$$\mathbf{F}_{ij}^K = \begin{cases} -\varepsilon_K \left[\frac{24}{d_m^{*7}} - \frac{48}{d_m^{*13}} \right] \cdot \hat{\mathbf{e}}_{ij} & d_m^* \leq d_{cu}^* \\ 0 & d_m^* > d_{cu}^* \end{cases} \quad (6)$$

In this equation $\hat{\mathbf{e}}_{ij}$ is the unit vector in the direction of the shortest distance from particle i to j .

The Hertzian elastic model can be write as [48]

$$\mathbf{F}_{ij}^H = \begin{cases} \varepsilon_H (1 - d_m^*)^{3/2} \cdot \hat{\mathbf{e}}_{ij} & d_m^* \leq 1 \\ 0 & d_m^* > 1 \end{cases} \quad (7)$$

with ε_H the strength of the Hertzian interaction, depending on the bacteria Young's modulus and size. This force is repulsive whenever there is an overlap between two bacteria, and zero in other cases. Figure 1-B shows the geometrical parameters involved in both models. Fig. 1-C shows the dependence of the different cell-cell interaction models on the minimum distance between cells. Comparing now the repulsive models of Kihara and Hertz, Fig. 1-C shows how at short overlaps between particles both models exert a similar repulsion (for equivalent values of the force intensity). At larger overlaps, the Hertz model is smoother, showing less repulsion than the Kihara model.

As shown in our previous studies [39, 57], the properties of microcolonies are highly dependent on the so-called Γ parameter, which summarises the competition between bacterial growth and bacterial diffusion. This parameter is defined as follows

$$\Gamma = \frac{t_{dif}}{t_{gr}} \quad (8)$$

Here t_{dif} is the average time required by an isolated particle of constant aspect ratio L_0^* to diffuse a distance σ by brownian diffusion, and t_{gr} the time need by an average bacterium to reach the aspect ratio L_f^* from its initial aspect ratio. For a given value of L_0^* , Γ is depending both on the diffusional parameter D_0 and on growth rate r . In the next section we will discuss the role of possible types of interaction between bacteria in different regimes characterised by different values of Γ . In each of these cases, to monitorize the evolution of the microcolony we have estimated de amount of biomass in

the microcolony, $m(t)$, defined as

$$m(t) = \sum_{i=1}^{N(t)} L_i^*(t) \quad (9)$$

being $N(t)$ the number of cells at time t . $m(t)$ is time-dependent because $N(t)$ and $L_i^*(t)$ vary over time.

To determine the shape and size of the microcolony, we have obtained the ellipse that best fits the distribution of particles. For this we have calculated the components of inertia tensor as

$$I_{\alpha,\beta} = \frac{1}{N(t)} \sum_{i=1}^{N(t)} \left(\delta_{\alpha,\beta} \left(\sum_{k=\alpha,\beta} r_i^k \right) - r_i^\alpha r_i^\beta \right) \quad (10)$$

Here α and β indicate the coordinates x or y , $\delta_{\alpha,\beta}$ is the Kronecker delta and r_i^α is the corresponding coordinate of the vector from the centre of mass of the microcolony to the position of the bacterium i . Diagonalizing this tensor is possible to calculate the two semi-axes, $a > b$, of the ellipse that best fit the distribution of bacteria in the microcolony [61]. From this calculation, the area covered by the micro-colony can be estimated as the area of these ellipses $A_e = \pi ab$. Therefore, the global density of the microcolony is calculated as $\rho(t) = m(t)/A_e(t)$. Moreover, the shape of the microcolony can be measured by the eccentricity. The square of this eccentricity is defined as follows:

$$e^2(t) = 1 - \frac{b^2}{a^2} \quad (11)$$

which approaches 0 for circular microcolonies. Additionally, to measure the orientational correlation of the particles the nematic order parameter $S_2(t)$ has been calculated by the standard procedure of diagonalizing a traceless symmetric tensor build with the orientation vectors of all the particles [57, 62, 63]. This nematic order parameter is 1 if all particles are parallel, and 0 if they are randomly oriented.

The value of ρ defined above provides global information on the compactness of the microcolony. To obtain information on the differences in the packing of bacteria in different areas of the biofilm, we have used the coverage profile $g_c(r_{cm})$. This function is defined as the fraction of the surface covered by bacteria at a distance r_{cm} from the microcolony center of mass. In the calculation of this function, a large number of random points are generated at a distance $r + dr$ from the centre of mass of the microcolony, evaluating $g_c(r_{cm})$ as the fraction of these points that fall in the area occupied by a bacterium.

As we have commented, the main goal of this work is to study how the characteristic of the option to model the interaction forces between bacteria influences the structural properties of the microcolony at different values of Γ . From our previous work [57], the different regimes in

biofilm evolution as a function of Γ values are known. Taking this previous information into account, we have selected as significant values of the whole range $\Gamma = 10, 1$ and 0.1 . To obtain these values, the growth rate has been chosen as $r \cdot \tau = 0.26, 0.026$ and 0.0027 , respectively, while keeping $D_0^* = 0.1$ in all cases. Specifying now for the interaction models used, for the repulsive Kirara model ($d_{cu} = \sqrt[3]{2}\sigma$) and the Kihara model with an attractive contribution ($d_{cu} = 2.5\sigma$), force intensities have been chosen in the interval $\varepsilon_K/k_B T \in [1, 100]$. In the case of the Hertz model, the force intensity changes in the interval $\varepsilon_H/(10^4 k_B T) \in [1, 100]$.

Throughout the simulations, the time step Δt has been limited to values less than $10^{-3}\tau$, while ensuring that at each step the displacement of the centre of mass of each cell was less than 0.01σ . For all the cases analysed in this work and in order to obtain statistical averages of the observables of interest, 500 independent trajectories were run, all starting with a single particle of aspect ratio L_0^* at the centre of the simulation box.

III. RESULTS

Biofilms are compact systems in which bacteria exert forces on each other. In real systems, this can lead to deformation of the cell walls. As the IbM models considered in this study are intrinsically rigid, this deformation is not considered. The equivalent consequence of the forces between bacteria in our algorithms would be the overlap between particles.

This overlap would result in distances between bacteria smaller than the cell diameter. These overlaps, which would be the equivalent of deformation in flexible models, will be unrealistic if they exceed a certain threshold. Therefore, a first indication of the realism, or the limitations, of each of the models at the different interaction intensities, would be to estimate the average overlap between particles. To quantify the magnitude of this overlap we have calculated the radial distribution function, $g(r)$. This distribution function gives information on how the structure around an average particle changes. This function is calculated as $g(r) \propto \langle \delta(r - |r_i - r_j|) \rangle$ [62], with the average being over all pairs of particles i and j . The position of the first peak of this function, r_1 , gives information about the average distance between nearest neighbours, thus obtaining information about the overlap between cells.

Fig. 2 shows the distance between first neighbours, r_1 , for all the models of force considered in this work as a function of the strength of the interaction and at the three values of Γ explored. All the values shown in this figure are obtained averaging over 500 independent configurations with value of biomass $m(t) = 2000$. As a first result for all models, the larger the Γ the smaller the average distance between the first neighbours. This is to be expected, since the higher the Γ the more compact the microcolony is [39, 57], and therefore the closer together

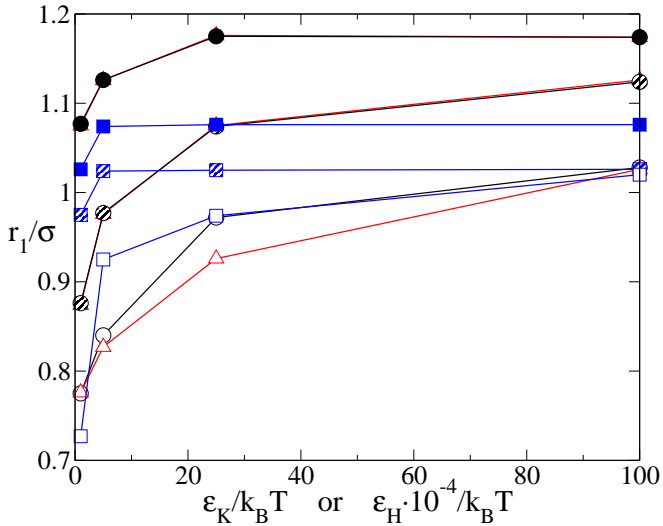


FIG. 2: Position of the first peak of the distribution function in units of bacterial diameter r_1/σ , for microcolonies with biomass $m(t) = 2000$ obtained with the repulsive Kihara model (black lines and circles), the attractive Kihara model (red lines and triangles) and the Hertz model (blue lines and squares) as a function of the interaction strength ($\varepsilon_K/k_B T$ for the Kihara models and $\varepsilon_H \cdot 10^{-4}/k_B T$ for Hertz). The cases with $\Gamma = 10$ (open symbols), 1 (dashed symbols) and 0.1 (solid symbols) are shown.

the particles are on average.

Focusing now in the case of $\Gamma = 10$, Fig. 2 shows as for low values of the strength of the interaction there is a high level of overlap between particles. This is dramatic in the case of the Hertz model with $\varepsilon_H = 10^4 k_B T$, for which r_1 is less than 0.75, indicating an average overlap of 25 percent of the cell radius between nearest neighbours. Both the attractive and repulsive Kihara models also show a significant level of overlap between particles, with r_1 less than 0.8 for $\varepsilon_K = 1 k_B T$.

In all models, as the strength of the interaction grows, the distance between the first neighbours also increases, notably the rapid increment of r_1 for the Hertz model. For stronger interactions there is a saturation in the value of r_1 , and the distance between first neighbours tends to a value independent of the intensity of the force. Thus, for example, in Kihara's models the first-neighbour distance changes little when ε_K changes from $25 k_B T$ to $100 k_B T$, as it does in Hertz's model when ε_H goes from $25 \cdot 10^4 k_B T$ to $100 \cdot 10^4 k_B T$. This confirms that this magnitude is quite independent at high values of the interaction intensity, maintaining the integrity of the cell membrane, and especially for the Hertz model. Interestingly, at intermediate values of the interaction strength, the attractive Kihara model shows a smaller distance between the closest neighbours r_1 than the other two repulsive models. This is a consequence of increased aggregation due to the attraction between cells. These differences between repulsive and attractive models disappear at higher values of

the interaction strength. Thus, at the highest values explored, and for $\Gamma = 10$, r_1 tends to 1.01 in all cases. This value indicates a small average overlap between bacteria, which is to be expected at this value of Γ where colonies tend to be very compact [39, 57].

Focusing now on the case of lower values of Γ , the dependence of r_1 on the interaction intensity shows a qualitative behavior similar to that described above, although with smaller values of r_1 . This indicates a low average overlap between cells, which is to be expected due to the lower compactness of the colonies. It is remarkable the coincidence at low values of Γ ($\Gamma = 1$ and 0.1) of the values of r_1 obtained for Kihara's attractive and repulsive models. This seems to indicate that, due to the higher relevance of bacterial diffusion at these values of Γ , possible attractive cell-cell interactions do not play a significant role. We will later qualify this conclusion by showing that at lower values of $m(t)$ the attractive character of the interaction does introduce differences. As in the case of $\Gamma = 10$, r_1 is almost independent of the interaction strength for intermediate and high values of ε_K and ε_H . In this range, the differences observed in Fig. 2 can be explained by the value of Γ (higher dispersion of cells for smaller Γ), and by the characteristics of the interaction model, with a longer repulsive tail for the Kihara models (see equations 6 and 7).

In conclusion, it can be seen from Fig. 2 that small values of the intensity of the interaction between bacteria lead to unrealistic situations, in which very high overlaps between bacteria occur. These overlaps could be observed, for instance, in the configuration obtained with the repulsive Kihara model with $\varepsilon_K = 1 k_B T$ for $\Gamma = 10$ at high value of the biomass (Fig. 1-D). In contrast, for this model and at this value of Γ but at higher strength of the interaction ($\varepsilon_K = 100 k_B T$, Fig. 1-E) the bacteria show greater separation from each other, being the lower crowding in this case apparent by visual inspection. Observing the configurations at low value of Γ ($\Gamma = 0.1$, with $\varepsilon_K = 1 k_B T$ and $100 k_B T$ in panels F and G of Fig. 1, respectively), it is not appreciate relevant different between them, confirmed the conclusions obtained from the analysis of position of first neighbours r_1 discussed up to now. It should be noted that these overlaps are not caused by the existence of attractive forces (there is an almost absolute coincidence between the attractive and repulsive models of Kihara at this value of $m(t)$), but by the internal pressures in the microcolony caused by the growth of the cells. Thus, the overlap is greater at higher values of Γ , where the colonies are more compact. In contrast, once a certain level of force strength is exceeded, this parameter has very little influence on the distance between first neighbours and on the overlap between near neighbours.

This increase in overlaps between particles at low value of strength intensity has relevant effects on some macroscopic properties. For example, the impact of overlap between particles is clear in colony density ($\rho\sigma^2$ in reduced units, Figure 3), where higher overlap values translate

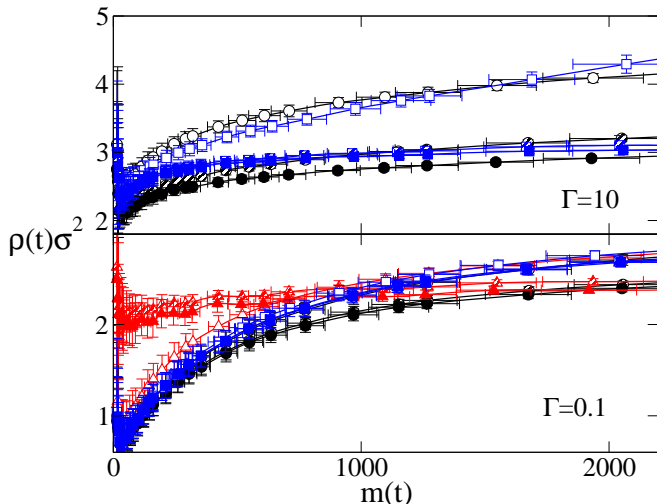


FIG. 3: Cell density in reduced units $\rho\sigma^2$ as function of the biomass $m(t)$ for $\Gamma = 10$ (top panel) and $\Gamma = 0.1$ (bottom panel). In both panels are represented results obtained with repulsive Kihara model (black lines and circles), attractive Kihara (red lines and triangles) and Hertz model (blue lines and squares). Open, dashed and solid symbols are for $\varepsilon_K = k_B T, 25k_B T$ and $100k_B T$ respectively in the case of Kihara models, and for $\varepsilon_H = 10^4 k_B T, 25 \cdot 10^4 k_B T$ and $100 \cdot 10^4 k_B T$ in the case of Hertz model.

into denser colonies. Fig. 3 shows that this change is more relevant at high values of Γ . Thus, for $\Gamma = 10$ (top panel of Fig. 3), the density $\rho\sigma^2$ in the case of the repulsive Kihara model with $\varepsilon_K = 1k_B T$ is much larger than for the other values of ε_K shown ($25k_B T$ and $100k_B T$). A similar trend is observed in the case of the Hertz model for the density obtained with the lower strength forces explored ($\varepsilon_H = 10^4 k_B T$) compared to the higher strength forces ($\varepsilon_H = 25 \cdot 10^4 k_B T$ and $100 \cdot 10^4 k_B T$), with values of the density similar to the obtained for Kihara's repulsive model. At this value of Γ the dependence of density on biomass in the case of the attractive Kihara model is coincident over the entire biomass range for a given value of ε_K with that described for the repulsive Kihara model. For this reason, data for this case have not been plotted in top panel of Fig. 3. Thus, for $\Gamma = 10$, the attractive and repulsive Kihara potentials have the same density values over the entire biomass range for a given value of ε_K . This indicates that, in compact colonies due to the competition between diffusion and growth [39, 57], the attractiveness of the interaction does not play a relevant role.

At intermediate and low values of Γ ($\Gamma = 1$ not shown, and $\Gamma = 0.1$, bottom panel of Fig. 3) the situation is very similar, but with some relevant qualitative differences. In any case, the bottom panel of Fig. 3 shows that the changes of the density values for the different potentials and forces studied are smaller than for $\Gamma = 10$. Within this smaller variation of the results, Fig. 3 indicates that for this value of Γ the trend is the same as the one men-

tioned for $\Gamma = 10$, so that the potentials presenting a higher overlap, measured with the value of r_1 shown in Fig. 1, induce the formation of microcolonies of higher density.

Despite the aforementioned, at this low value of Γ an important qualitative difference is observed in the case of Kihara's attractive potential. Thus, when the strength in this model is sufficiently intense ($\varepsilon_K = 25k_B T$ and $100k_B T$), at low values of biomass a different behavior is observed than in the repulsive models. Whereas for low and intermediate values of biomass, $\rho\sigma^2$ shows higher values for the attractive models with high interactions than for the repulsive Kihara or Hertz potentials. At higher values of $m(t)$ and in this range of force intensity, the density in all models is similar, something expected from the coincidence of the value of r_1 among these models for $m(t) = 2000$ discussed in Fig. 2. This phenomenology is indicating that, although at this low value of Γ bacterial diffusion dominates over growth and cells tend to disperse on the surface, if attractive interactions are sufficiently intense, dispersal is slowed by attraction between cells, which favour their staying together. Thus, although attractive interactions do not seem to play a relevant role when the colony is compact, it is relevant in situations where without these attractive interactions cells would trend to disperse.

In summary, the results discussed up to now confirm the general behavior obtained in previous studies [39, 57], which indicated that denser microcolonies are formed at higher Γ values. But we see that this density depend also on the model and, above all, the strength of the interaction between cells. Thus, low interactions result in high densities, as overlapping between bacteria becomes possible. Conversely, more intense repulsive interactions between bacteria result in lower density values. This has consequences for the value of other macroscopic quantities that depend on density. For example, previous studies [39, 57] shown that higher density values result in more ellipsoidal colonies (higher eccentricity values), and with higher orientational order (higher value of the nematic order parameter).

Fig. 4 confirms this dependence in the case of $\Gamma = 10$. In this case (panels A and C) it can be seen that the lower the force intensity, and therefore the cell density, the higher the eccentricity and the nematic order parameter for the different models. In any case it is not a very strong dependence, and with all intensities the same conclusions would be reached as in previous work. At low values of Γ (0.1 in panels B and D for $e^2(t)$ and $S_2(t)$) the results are very independent of the force model and intensity, confirming that in non-compact colonies this is not a relevant factor.

Further insight into this influence can be gleaned from analysing the behaviour of the coverage profile $g_c(r_{cm})$ as a function of the distance to the centre of mass of the microcolony r_{cm} . Thus, Fig. 5 shows this function for the force models and strength explored in this study, for $\Gamma = 10$ and 0.1, at three values of biomass

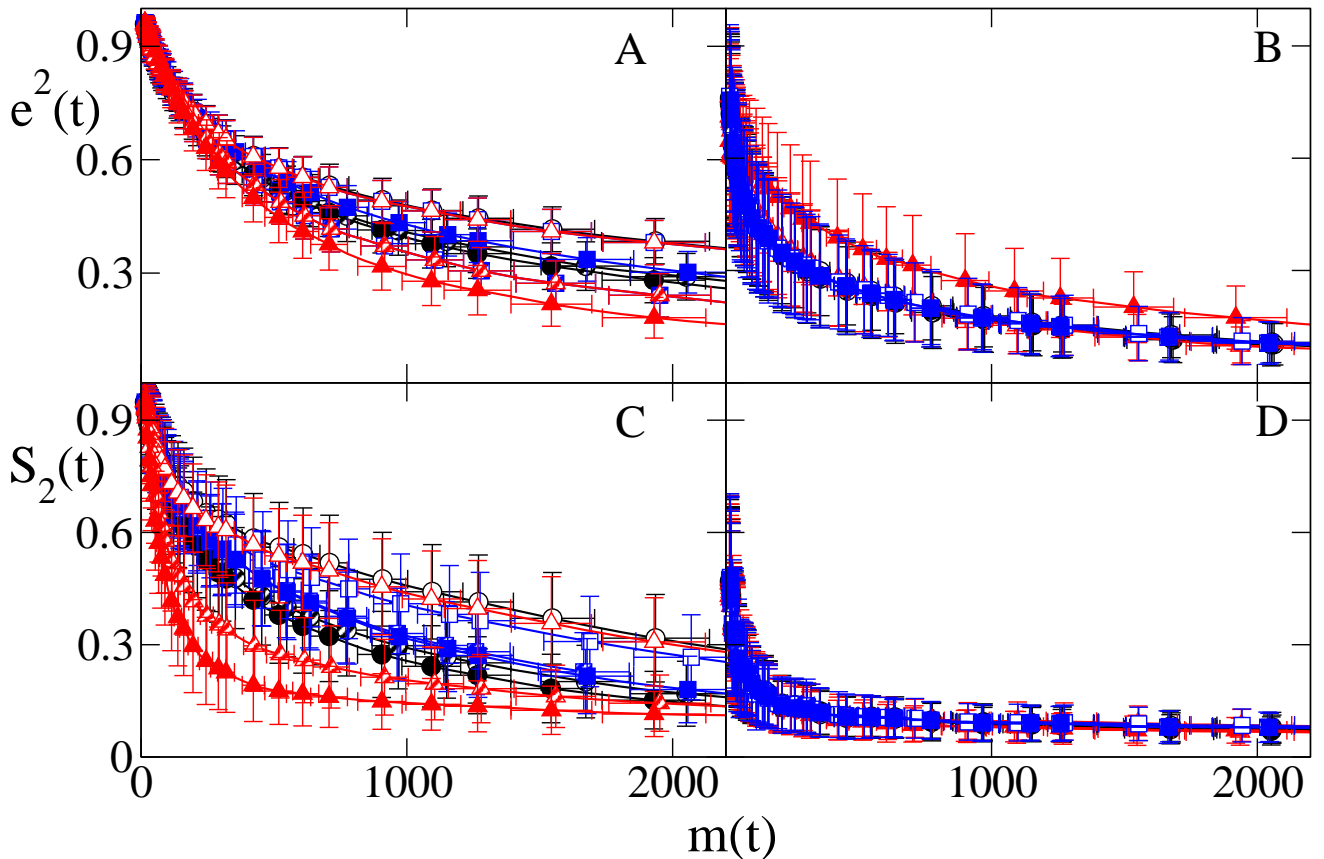


FIG. 4: Square of the eccentricity of the microcolony ($e^2(t)$) and nematic order parameter ($S_2(t)$) as a function of the biomass $m(t)$, for $\Gamma = 10$ (A) and (C), and for $\Gamma = 0.1$ (B) and (D). The results obtained with repulsive Kihara, attractive Kihara and Hertz models are represented by the same symbols than in Fig. 3.

($m(t) = 100, 500, 2000$) representing three stages in the development of microcolonies. The trends we observed in the behaviour of g_c can be explained with the same arguments previously used for density, order parameter or eccentricity. Thus, at $\Gamma = 10$ (top row of Fig. 5), for all the models studied, the microcolony is more compact the lower the strength of the interaction between cells. This effect is clearer as the biomass grows. In contrast, for higher interaction strengths these differences between coverings for different models and strengths tend to disappear.

It is noteworthy that at the lowest biomass value and for $\Gamma = 0.1$, the fraction of coverage is higher in the case of potentials with an attractive component than in the rest. This difference is magnified in the case of the attractive Kihara potentials with the high strength ($\varepsilon_K/k_B T = 25$ and 100), where values for g_c close to 0.6 are reached in the centre of the microcolony, while the rest of the models do not exceed 0.4. At higher values of biomass and other values of Γ these differences do not appear, and the values of g_c for the attractive Kihara models are similar as for the repulsive models with the same value of ε_K . The values of g_c at these values of $m(t)$ and Γ are also quite similar to those obtained with the Hertz model. This

confirms the relevance of attractive models in situations where cells are dispersed on the surface, forming structures more similar to swarms than to biofilms, but their loss of importance in situations where aggregate structures are formed (high values of $m(t)$ and Γ). Apart from this specific behaviour for the attractive potential, the changes in g_c can also be systematized from the measurement of the inter-particle overlap discussed in Fig. 2, with lower coverage in the central zone the higher the inter-particle overlap. At the edge of the microcolony this lower coverage translates into an enlargement of the microcolony size. The latter effect is more evident the higher the biomass value.

Therefore, we have observed how the strength of the forces between bacteria can play an important role in modelling some of the properties of the biofilm. So far we have focused this discussion on the structural properties that have already been discussed in previous works (which focus solely on the repulsive Kihara model). It will be interesting at this point to analyse the effect on other mechanical properties, which a priori would be more related to the force model. For this purpose, we characterize the stress that the particles undergo due to interaction with neighboring cells. To do this, we have

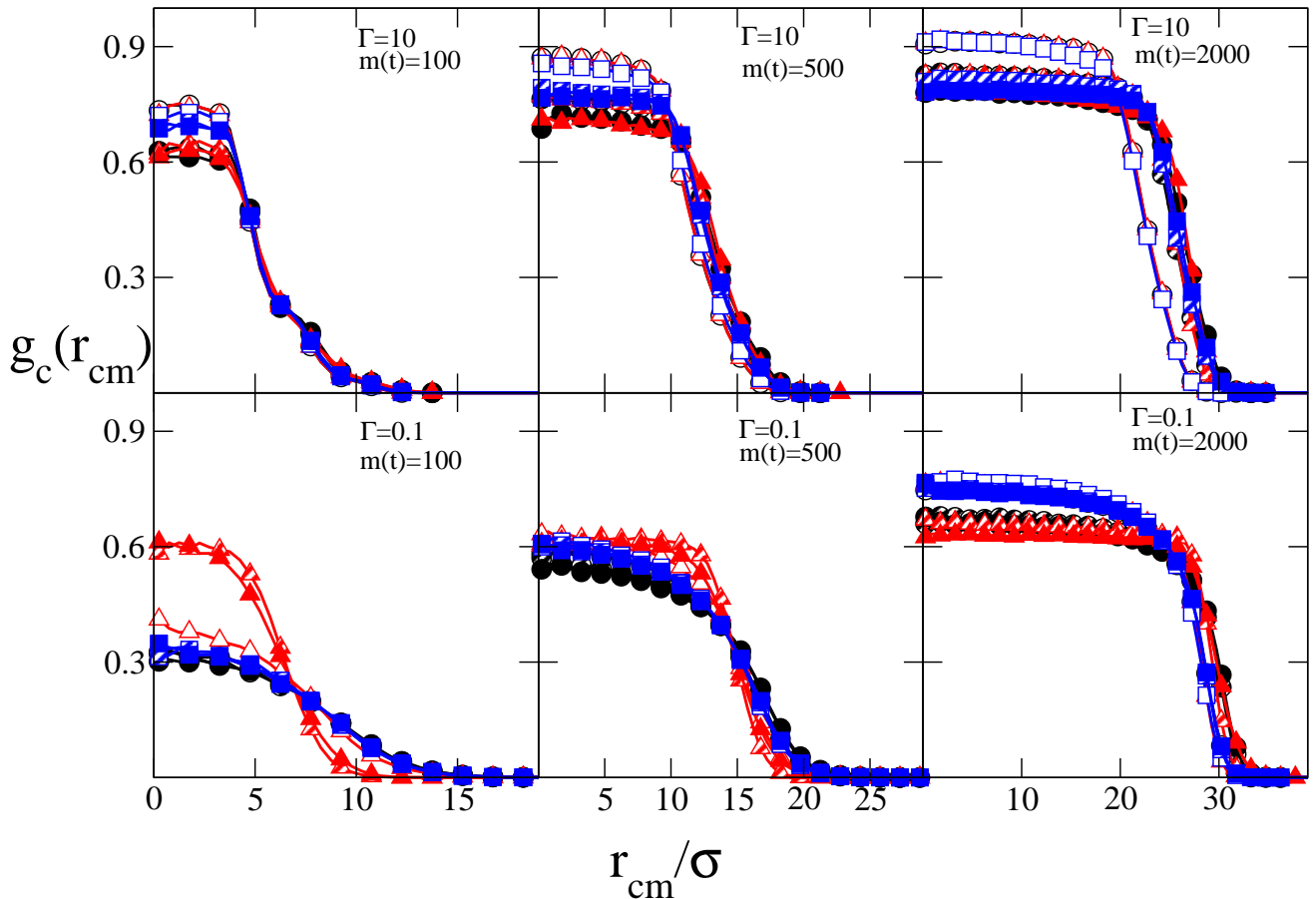


FIG. 5: Surface coverage profiles $g(r_{cm})$ for microcolonies with $m(t) = 100, 500$ and 2000 (left, middle and right column, respectively), and $\Gamma = 10$ and 0.1 (top and bottom row, respectively) obtained with repulsive Kihara model (black lines and circles), attractive Kihara (red lines and triangles) and Hertz model (blue lines and squares). Open, dashed and solid symbols are for $\varepsilon_K = k_B T, 25k_B T$ and $100k_B T$ respectively in the case of Kihara models, and for $\varepsilon_H = 10^4 k_B T, 25 \cdot 10^4 k_B T$ and $100 \cdot 10^4 k_B T$ respectively in the case of Hertz model.

calculated the dimensionless stress tensor on particle i as

$$p_{\alpha,\beta}^i = \frac{-1}{V_i} \frac{\sigma^3}{k_B T} \sum_{j=1}^{N_c} \mathbf{r}_{\alpha}^{i_j} \cdot \mathbf{F}_{\beta}^{i_j} \quad (12)$$

where V_i is the volume of bacterium i and the sum is performed for all N_c bacteria j at a distance from bacterium i less than the interaction cut-off. $\mathbf{r}_{\alpha}^{i_j}$ is α component of the position vector of the contact point between i and j from the centre of cell i and $\mathbf{F}_{\beta}^{i_j}$ is the β component of the force exerted by j over i . The hydrostatic (and isotropic) pressure that a cell undergoes due to the interaction with the surrounding bacteria can be obtained from the trace of this tensor $p_0^i = 1/2(p_{x,x}^i + p_{y,y}^i)$. From the definition of Eq. 12, p_0 is defined as a dimensionless quantity. In Fig. 6 we show the average of this pressure for all cells at the same distance from the colony's centre of mass, $p_0(r_{cm})$, as a function of this distance. Thus, this graph shows the pressure that a cell suffers as a func-

tion of its position within the colony. We show in this figure the results for microcolonies in advanced stages, with $m(t) = 2000$, for the extreme Γ values considered in this study ($\Gamma = 10$ in the upper panel and 0.1 in the lower panel) and for all the models and intensities discussed above.

The behavior of p_0 at this value of biomass shows a general dependence on r_{cm} , regardless of the value of Γ . Thus, in both panels of Fig. 6 it can be seen how p_0 shows a high pressure plateau in the centre of the microcolony, with a decrease from here towards the edge. In any case, this plateau is narrow, and a general feature is the inhomogeneity in the pressure felt by the cells within the microcolony. This dependence has been reported by other authors in the past for tissues [23] and bacteria [48].

Focusing now on the dependence of p_0 on Γ , the comparison of both panels of Fig. 6 allows us to establish that, the larger Γ is, the higher values p_0 reaches. Thus, although in the cases shown in the figure the aforementioned trends in the dependence of p_0 on the position in the microcolony are maintained, the values obtained for

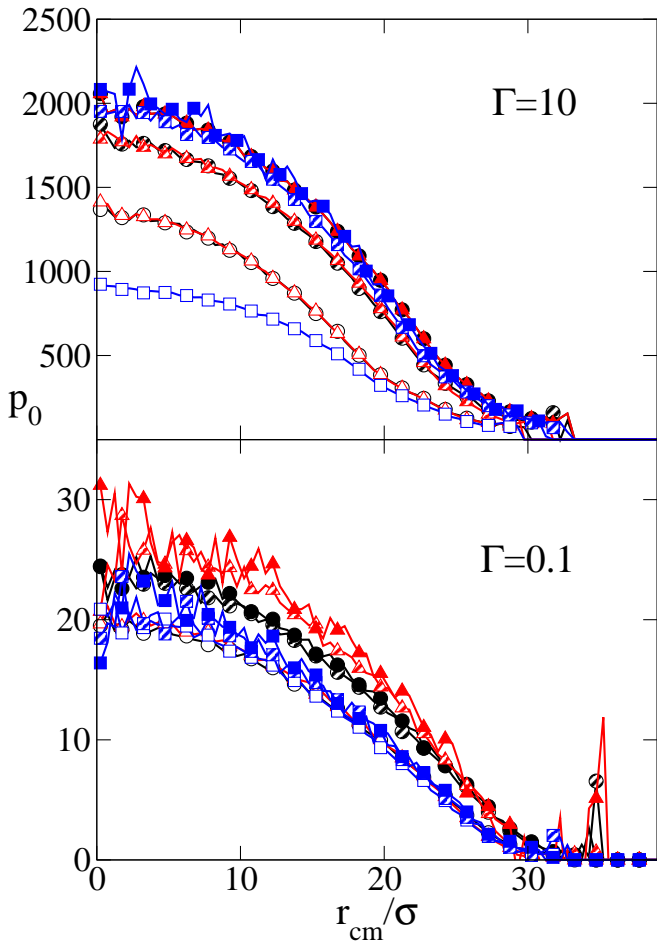


FIG. 6: Profile of the isotropic dimensionless pressure p_0 felt by bacteria depending on the position respect to the centre of mass of the biofilm r_{cm} at biomass $m(t) = 2000$ for $\Gamma = 10$ (top panel) and 0.1 (bottom panel), obtained with repulsive Kihara model (black lines and circles), attractive Kihara (red lines and triangles) and Hertz model (blue lines and squares). Open, dashed and solid symbols are for $\varepsilon_K = k_B T, 25k_B T$ and $100k_B T$ respectively in the case of Kihara models, and for $\varepsilon_H = 10^4 k_B T, 25 \cdot 10^4 k_B T$ and $100 \cdot 10^4 k_B T$ in the case of Hertz model.

each case show an important variation. Thus, for $\Gamma = 10$ the pressure in the centre can reach values around 1500, for $\Gamma = 0.1$ it reaches levels between 20 and 30, respectively. These differences in the pressure felt by the cells for each value of Γ are related to the compactness of the microcolony, higher the higher the Γ due to the lower cell diffusion with respect to growth in this case, and the increase in density (Fig. 2) and thus the interaction between bacteria. Surprisingly, the influence of model and force intensity is not as apparent as in previous observable. This is very clear when comparing the repulsive Kihara models. For $\Gamma = 10$ it is found that an increase of $\varepsilon_K = 1$ to 100 only means an increase of about two times in the pressure at the centre of the colony (from about 1200 to 2000). This change is even smaller for $\Gamma = 1$ (from 175 to 250, not shown) and almost non-existent

for $\Gamma = 0.1$.

Regarding the comparison between models, Kihara's attractive and repulsive models coincide in the quantitative and qualitative behaviour of this magnitude at this amount of biomass for $\Gamma = 10$. This was expected given the coincidence of the values of other observables for these two models at high biomass values. Interestingly, for $\Gamma = 0.1$ p_0 is higher for the attractive Kihara model than for the repulsive one. This is another indication that the attractive interaction might be more relevant in less crowded situations. For the Hertz models of different strength, p_0 follows a qualitative and quantitative behaviour similar to that found for the repulsive Kihara model, as can be seen in Fig. 6.

IV. DISCUSSION AND FINAL REMARKS

In summary, in this work we have addressed, through extensive simulations under different conditions, the relevance of the choice of force model when simulating the development of bacterial biofilms using agent-based models. A study like this is relevant because there is not much information on direct experimental measurements of the force between two cells as a function of their shape, size or relative distance. Therefore, the models chosen in the different studies available in the literature are extrapolations of models developed in other fields, such as elastic materials or colloidal systems [37]. In the absence of direct measurements, the realism and goodness of the models used must be validated indirectly through the characteristics of the cell colonies obtained by simulation.

From our results we conclude that, although there are differences when using one model or another, for example the repulsive or attractive models of Kihara or Hertz in our work, the factor with the most influence on the structural properties of the biofilm is the intensity of the interaction between the cells, rather than how these forces are modelled. Thus, low strengths of the interaction forces favour the appearance of very high overlaps between the cells, which are to be considered unrealistic. When the strength of the forces is increased, these overlaps are reduced and eventually disappear. From a certain threshold of this strength, the results begin to be independent of the parameter that controls the strength of the force, and even of the force model itself that is being applied.

From the results presented here, it is deduced that there is a correlation between the choice of the model for the forces between the cells and their intensity and some of the properties obtained from the growing colonies. These correlations can be explained by the level of overlap between the particles observed for the different cases. For example, the density of the colony is higher the higher the level of overlap between particles, which is relevant for low force intensities. This variation in density translates into other indicators of colony shape such as eccentricity or internal order such as the nematic order parameter, which previous works [39, 57] have shown to be

strongly dependent on the level of compactness of the colony. But in any case it does not seem to be a particularly relevant effect, and for example a variation of two orders of magnitude in the intensity of the forces causes a much smaller change in these magnitudes, the effect of other parameters such as Γ being more relevant. An example of this limited influence is the value of the pressure that the bacteria suffer from being in the centre of the colony. One would expect this magnitude to have a direct relationship with the increase in force intensity, however the influence is much milder, with only a doubling of the increase when the intensity increases by two orders of magnitude. However, taking into account the high Young's modulus reported in several works [50] for the interaction between bacteria, and the independence of the results when the intensity of the forces increases, it seems advisable to use these high values for modelling the growth of bacterial colonies. We refer to values higher than $25k_B T$ for Kihara models, and higher than $25 \cdot 10^4 k_B T$ for the case of the Hertz model.

The existence of an attractive contribution to the interaction between bacteria deserves a separate mention. It follows from our results that this possible attractive interaction is only relevant in situations where the colony is not very compact. This means small Γ values (situations where diffusion is high and dominant versus cell growth and division), and low biomass values. That is, when cells are initially separated and have not yet

filled the space by cell reproduction. In other cases, situations with high Γ values where colonies are compact from the early stages, or in more mature colonies with higher biomass, the results found are fully equivalent to those of purely repulsive models. This conclusion follows from the comparison of the attractive and repulsive Kihara models. It should be noted that this comparison could be made with other models, for example by comparing the repulsive Hertz model studied in this paper with the Johnson-Kendall-Roberts contact model, which is a modification of the Hertz model by introducing an attractive [64–66] contribution. We believe that, in any case, the conclusions would be the same as those found in the comparison of the attractive and repulsive Kihara models, and that this additional comparison would not provide qualitatively different results.

Acknowledgments

This work was supported by the Spanish Ministerio de Ciencia e Innovación and FEDER (Projects n. PID2021-126121NB-I00)/CHU A.R.R. acknowledges financial support from Grant No. PID2021-126348NB-I00 funded by MCIN/AEI/10.13039/501100011033. We thank C3UPO for the HPC facilities provided.

-
- [1] J. G. Gay and B. J. Berne, *J. Chem. Phys.* **74**, 3316 (1981).
- [2] E. D. Miguel, L. F. Rull, M. K. Chalam, and K. E. Gubbins, *Mol. Phys.* **74**, 405 (1991).
- [3] L. F. Rull, *Physica A: Statistical Mechanics and its Applications* **220**, 113 (1995), ISSN 0378-4371.
- [4] S. C. McGrother, D. C. Williamson, and G. Jackson, *J. Chem. Phys.* **104**, 6755 (1996).
- [5] P. Bolhuis and D. Frenkel, *J. Chem. Phys.* **106**, 666 (1997).
- [6] T. Kihara, *Rev. Mod. Phys.* **25**, 831 (1953).
- [7] A. Cuetos, B. Martínez-Haya, S. Lago, and L. F. Rull, *J. Phys. Chem. B* **109**, 13729 (2005).
- [8] B. Martínez-Haya, A. Cuetos, S. Lago, and L. F. Rull, *J. Chem. Phys.* **122**, 024908 (2005).
- [9] J. W. Costerton, Z. Lewandowski, D. E. Caldwell, D. R. Korber, and H. M. Lappin-Scott, *Annu. Rev. Microbiol.* **49**, 711 (1995).
- [10] H. C. Flemming, J. Wingender, U. Szewzyk, P. Steinberg, S. A. Rice, and S. Kjelleberg, *Nat. Rev. Microbiol.* **14**, 563 (2016).
- [11] Y. F. Dufrêne and A. Persat, *Nat. Rev. Microbiol.* **18**, 227 (2020).
- [12] T. Ishikawa, T. Omori, and K. Kikuchi, *APL Bioeng.* **4**, 041504 (2020).
- [13] A. Persat, C. Nadell, M. Kim, F. Ingremeau, A. Siryaporn, K. Drescher, N. Wingreen, B. Bassler, Z. Gitai, and H. Stone, *Cell* **161**, 988 (2015).
- [14] J. Dunkel, S. Heidenreich, K. Drescher, H. H. Wensink, M. Bär, and R. E. Goldstein, *Phys. Rev. Lett.* **110**, 228102 (2013).
- [15] S. Geisel, E. Secchi, and J. Vermant, *Interface Focus* **12**, 20220032 (2022).
- [16] J. Martín-Roca, V. Bianco, F. Alarcón, A. K. Monnappa, P. Natale, F. Monroy, B. Orgaz, I. López-Montero, and C. Valeriani, *J. Chem. Phys.* **158**, 074902 (2023).
- [17] L. Pavlovsky, R. A. Sturtevant, J. G. Younger, and M. J. Solomon, *Langmuir* **31**, 2036 (2015).
- [18] M. Delarue, J. Hartung, C. Schreck, P. Gniewek, L. Hu, S. Herminghaus, and O. Hallatschek, *Nat. Phys.* **12**, 762 (2016).
- [19] B. Alric, C. Formosa-Dague, E. Dague, L. J. Holt, and M. Delarue, *Nat. Phys.* **18**, 411 (2022).
- [20] P. S. Stewart and C. R. Robertson, *Appl. Microbiol. Biotechnol.* **30**, 34 (1989).
- [21] D. Volfson, S. Cookson, J. Hasty, and L. S. Tsimring, *Proc. Natl. Acad. Sci. USA* **105**, 15346 (2008).
- [22] L. A. Genova, M. F. Roberts, Y.-C. Wong, C. E. Harper, A. G. Santiago, B. Fu, A. Srivastava, W. Jung, L. M. Wang, Łukasz Krzemiński, et al., *Proc. Natl. Acad. Sci. USA* **116**, 25462 (2019).
- [23] B. I. Shraiman, *Proc. Natl. Acad. Sci. USA* **102**, 3318 (2005).
- [24] M. Valet, E. D. Siggia, and A. H. Brivanlou, *Nat. Rev. Mol. Cell Biol.* **23**, 169 (2022).
- [25] G. Helmlinger, P. A. Netti, H. C. Lichtenbeld, R. J. Melder, and R. K. Jain, *Nat. Biotechnol.* **15**, 778 (1997).
- [26] K. Alessandri, B. R. Sarangi, V. V. Gurchenkov,

- B. Sinha, T. R. Kießling, L. Fetler, F. Rico, S. Scheuring, C. Lamaze, A. Simon, et al., *Proc. Natl. Acad. Sci. USA* **110**, 14843 (2013).
- [27] A. Persat, *Curr. Opin. Microbiol.* **36**, 1 (2017).
- [28] V. D. Gordon and L. Wang, *J. Cell Sci.* **132**, jcs227694 (2019).
- [29] C. Even, C. Marlière, J.-M. Ghigo, J.-M. Allain, A. Marcellan, and E. Raspaud, *Adv. Colloid Interface Sci.* **247**, 573 (2017).
- [30] X. Jin and J. S. Marshall, *Phys. Fluids* **32**, 091902 (2020).
- [31] P. Aprikian, G. Interlandi, B. A. Kidd, I. Le Trong, V. Tchesnokova, O. Yakovenko, M. J. Whitfield, E. Bullitt, R. E. Stenkamp, W. E. Thomas, et al., *PLoS Biol.* p. e1000617 (2011).
- [32] L. D. Renner and D. B. Weibel, *MRS Bull.* **36**, 347 (2011).
- [33] Q. Wang and T. Zhang, *Solid State Commun.* **150**, 1009 (2010).
- [34] P. A. Dzianach, G. A. Dykes, N. J. C. Strachan, K. J. Forbes, and F. J. Pérez-Reche, *Journal of The Royal Society Interface* **16**, 20190042 (2019).
- [35] M. Aghajani Delavar and J. Wang, *Advanced Methods and Mathematical Modeling of Biofilm* (2022), ISBN 9780323903745.
- [36] J.-U. Kreft, C. Picioreanu, J. W. T. Wimpenny, and M. C. M. van Loosdrecht, *Microbiology* **147**, 2897 (2001).
- [37] G. W. Jones and S. J. Chapman, *SIAM Rev.* **54**, 52 (2012).
- [38] P. Van Liedekerke, M. M. Palm, N. Jagiella, and D. Drasdo, *Comput. Part. Mech.* **2**, 401 (2015).
- [39] R. D. Acemel, F. Govantes, and A. Cuetos, *Sci. Rep.* **8**, 5340 (2018).
- [40] J. Nijjer, C. Li, M. Kothari, T. Henzel, Q. Zhang, J.-S. B. Tai, S. Zhou, T. Cohen, S. Zhang, and J. Yan, *Nature Physics* **19**, 1936 (2023).
- [41] A. I. Hochbaum and J. Aizenberg, *Nano Lett.* **10**, 3717 (2010).
- [42] A. Epstein, A. Hochbaum, K. Philseok, and J. Aizenberg, *Nanotechnology* **22**, 494007 (2011).
- [43] D. Drasdo and M. Loeffler, *Nonlinear Analysis: Theory, Methods & Applications* **47**, 245 (2001).
- [44] D. Stekel, R. J., and E. D. Williams, *J. Theor. Biol.* **175**, 283 (1995).
- [45] E. Palsson and H. G. Othmer, *Proc. Natl. Acad. Sci. USA* **97**, 10448 (2000).
- [46] L. Landau and E. Lifschitz, *Theory of elasticity* (Elsevier, Oxford, UK, 2008), 3rd ed.
- [47] M. Doumic, S. Hecht, and D. Peurichard, *Mathematical Biosciences and Engineering* **17**, 6873 (2020).
- [48] Z. You, D. J. G. Pearce, A. Sengupta, and L. Giomi, *Phys. Rev. X* **8**, 031065 (2018).
- [49] M. A. A. Grant, B. Waclaw, R. J. Allen, and P. Cicuta, *J. R. Soc. Interface* **11**, 20140400 (2014).
- [50] H. H. Tuson, G. K. Auer, L. D. Renner, M. Hasebe, C. Tropini, M. Salick, W. C. Crone, A. Gopinathan, K. C. Huang, and D. B. Weibel, *Mol. Microbiol.* **84**, 874 (2012).
- [51] D. J. Eartl, J. Ilnytski, and M. R. Wilson, *Mol. Phys.* **99**, 1719 (2001).
- [52] A. Cuetos, B. Martínez-Haya, L. F. Rull, and S. Lago, *J. Chem. Phys.* **117**, 2934 (2002).
- [53] A. Cuetos and B. Martínez-Haya, *Mol. Phys.* **113**, 1137 (2015).
- [54] A. Cuetos, B. Martínez-Haya, S. Lago, and L. F. Rull, *Phys. Rev. E* **68**, 011704 (2003).
- [55] F. J. Lobo-Cabrera, A. Patti, F. Govantes, and A. Cuetos, *Phys. Rev. E* **103**, 052407 (2021).
- [56] F. J. Lobo-Cabrera, T. Navarro, A. Iannini, F. Casares, and A. Cuetos, *Front. Cell Dev. Biol.* **9**, 681933 (2021).
- [57] A. Delgado-Campos and A. Cuetos, *Phys. Rev. E* **106**, 034402 (2022).
- [58] C. Vega and S. Lago, *J. Chem. Phys.* **93**, 8171 (1990).
- [59] J. Bonet Avalos, J. Rubí, D. Bedeaux, and G. van der Zwan, *Physica A: Statistical Mechanics and its Applications* **211**, 193 (1994).
- [60] C. Vega and S. Lago, *Comput. Chem.* **18**, 55 (1994).
- [61] R. A. Karnesky, C. K. Sudbrack, and D. N. Seidman, *Scr. Mater.* **57**, 353 (2007).
- [62] M. P. Allen, G. T. Evans, D. Frenkel, and B. M. Mulder, in *Advances in chemical physics* (Wiley Online Library, 2007), vol. 86, pp. 1–166.
- [63] A. A. Mercurieva and T. M. Birshtein, *Macromol. Theory Simul.* **1**, 205 (1992).
- [64] D. Xu, E. Kaliviotis, A. Munjiza, E. Avital, C. Ji, and J. Williams, *Journal of Biomechanics* **46**, 1810 (2013).
- [65] R. Spolenak, S. Gorb, H. Gao, and E. Arzt, *Proceedings Of The Royal Society A-Mathematical Physical And Engineering Sciences* **461**, 305 (2005), ISSN 1364-5021.
- [66] W. Zhang, A. G. Stack, and Y. Chen, *Colloids And Surfaces B-Biointerfaces* **82**, 316 (2011).